Supporting Information

Hierarchical NC/Ni-CoP Nanoarrays Supported on Nickel Foam: Synergistic Electronic Modulation and Surface Reconstruction for High-Efficiency Ethanol Oxidation

Zhiwei Wei[1], Obeylaw Moyo[1], Mujia Sun[1], Jiaqiao Yang[1], Jiqiang Ding[1], Xi Wu[1], Junxiong Zhang[2,*], Hainan Sun[1,*]

[1] School of Chemistry and Chemical Engineering, Nantong University, Nantong, 226019, China

[2] School of Textile and Clothing, Nantong University, Nantong, 226019, China

*E-mail: zhangjunxiong@ntu.edu.cn (J. Zhang); hainansun123919@ntu.edu.cn (H. Sun)

Experimental Procedures

Chemicals and Reagents.

Nickel Foam (NF), hydrochloric acid, ethanol, and deionized water were used in all of the experiments. Cobalt chloride ($CoCl_2 \cdot 6H_2O$, ACS, ≥98%), nickel chloride ($NiCl_2 \cdot 6H_2O$, ACS, ≥99.9%), urea (CH_4N_2O, ACS, ≥99.5%), ammonium fluoride (NH_4F, ACS, ≥98.0%), 2-methylimidazole ($C_4H_6N_2$, ≥98.0%), potassium hydroxide (KOH, ACS, ≥85.0%) and ethanol (C_2H_5OH, AR, ≥95%) were purchased from Aladdin Chemistry Co., Ltd. (Beijing, China). Sodium hypophosphite (NaH_2PO_2, 98.0%) was supplied by Bide Pharmatech Co., Ltd. (Shanghai, China).

Synthesis of Ni-Co LDH/NF, ZIF-67/Ni−Co LDH/NF, and NC/Ni-CoP/NF.

Prior to use, nickel foam (NF, 4 × 3 cm^2) was pretreated to remove surface oxides by immersion in 1 M HCl for 10 min, followed by rinsing with deionized (DI) water for 5 min and ultrasonication in ethanol for 15 min. The cleaned NF was then dried in a vacuum oven overnight. Subsequently, 3.2 mmol $CoCl_2 \cdot 6H_2O$, 0.8 mmol $NiCl_2 \cdot 6H_2O$, 20 mmol urea, and 16 mmol NH_4F were dissolved in 60 mL DI water and stirred for 30 min. The solution was transferred into a 100 mL Teflon-lined stainless-steel autoclave, and the pretreated NF was immersed in the precursor solution. The autoclave was maintained at 120 °C for 5 h. After cooling, the sample was washed with DI water and dried overnight under vacuum to obtain Ni–Co LDH/NF. For ZIF-67 coating, the as-prepared Ni-Co LDH/NF (3 × 2 cm^2) was immersed in a homogeneous solution containing 1.64 g 2-methylimidazole dissolved in 5 mL DI water and 5 mL ethanol for 12 h at room temperature, yielding ZIF-67/Ni-Co LDH/NF. Phosphorization was carried out by placing ZIF-67/Ni-Co LDH/NF in a porcelain boat together with 0.5 g NaH_2PO_2, followed by annealing at 300 °C for 1 h to obtain NC/Ni-CoP/NF. Ni-CoP/NF was prepared using the same procedure without the ZIF-67 coating step. NC/CoP/NF was synthesized by omitting $NiCl_2 \cdot 6H_2O$, while CoP/NF was obtained under similar conditions without both Ni precursor and ZIF-67 coating. NC/NiP/NF and NiP/NF were prepared analogously using only the Ni precursor, with NiP/NF further excluding both the ZIF-67 coating and hydrothermal growth steps.

Characterizations.

X-ray diffraction (XRD) patterns were collected on a Rigaku D8 diffractiometer. The morphology of the catalysts was characterized using scanning electron microscopy (SEM, JEOL JSM-6700F) and transmission electron microscopy (TEM, JEOL ARM-200FTH). High-resolution X-ray photoelectron spectroscopy (XPS) measurements were conducted on the Thermo Scientific Escalab 250 Xi under ultra-high vacuum conditions (< 10^{-6} bar).

Electrochemical Measurements

Electrochemical measurements were carried out using a CS2350M bipotentiostat (Corrtest, Wuhan, China) in a standard three-electrode configuration. A Hg/HgO electrode was used as the reference electrode, and a graphite rod served as the counter electrode. Linear sweep voltammetry (LSV) was conducted at a scan rate of 5 mV s^{-1}, and all potentials were corrected for *iR* compensation. The potentials were converted to the reversible hydrogen electrode (RHE) scale according to:

$E_{RHE} = E_{Hg/HgO} + 0.925 - iR_{solution}$.

Cyclic voltammetry (CV) was performed at various scan rates (10, 15, 20, 25, and 30 mV s^{-1}) to estimate the double-layer capacitance (*Cdl*) of the catalysts. Electrochemical impedance spectroscopy (EIS) measurements were carried out over a frequency range from 0.01 Hz to 100 kHz. Long-term stability was evaluated by chronopotentiometric measurements. All measurements were conducted in 1 M KOH containing 1 M ethanol unless otherwise stated. The Faradaic efficiency (FE) for acetate formation during ethanol oxidation was determined by comparing the experimentally measured acetate concentration with the theoretical amount calculated from the total charge passed during electrolysis. The acetate concentration was quantified using a calibration curve constructed from standard acetate solutions with concentrations of 0.01, 0.02, 0.05, 0.10, and 0.15 M, which showed excellent linearity (R^2 = 0.998). The total amount of acetate produced was calculated based on the measured concentration and the total electrolyte volume (80 mL). The FE was calculated according to the following equation:

$$FE = \frac{n \times F \times N_{acetate}}{Q} \times 100\%$$

where n = 4 is the number of electrons involved in the ethanol-to-acetate oxidation pathway, F is the Faraday constant (96485 C mol^{-1}), $N_{acetate}$is the number of moles of acetate produced, and Q is the total charge passed during electrolysis.

Operando Raman Spectroscopy.

Operando Raman was conducted using a three-electrode Raman cell was used for the measurements. The applied potential was maintained for 90 s before each measurement to ensure its equilibrium state. For the measurements, 1 M KOH and 1 M ethanol was used as the electrolyte. The acquisition time was set to 5 s, and complete spectra were acquired by averaging 10 scans.

Differential Electrochemical Mass Spectrometry (DEMS).

DEMS (QAS100, Shanghai Linglu Instrument) combined with an electrochemical workstation (Corrtest, Wuhan, China) was employed in a typical three-electrode electrochemical cell. 1 M KOH with 1 M ethanol was used as the electrolyte. The working electrode was paved on a porous PTFE membrane, where the hydrophobic PTFE membrane permits gas flow while rejecting liquid. To trap the water vapour for averting potential damages to the mass spectrometer, a cold trap cooled with dry ice was installed between the electrochemical cell and the vacuum chamber. CV scan was conducted with a scan rate of 5 mV s^{-1} over a potential range of 1.0 to 1.45 V vs. RHE, while recording the mass signals m/z of different volatile products.

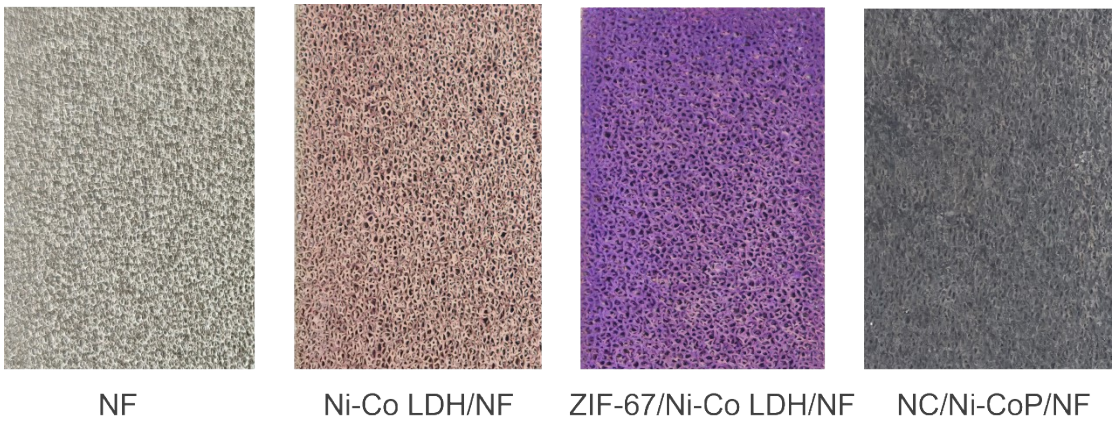

Fig. S1. Photographs showing the color evolution during the synthesis of NC/Ni-CoP/NF.

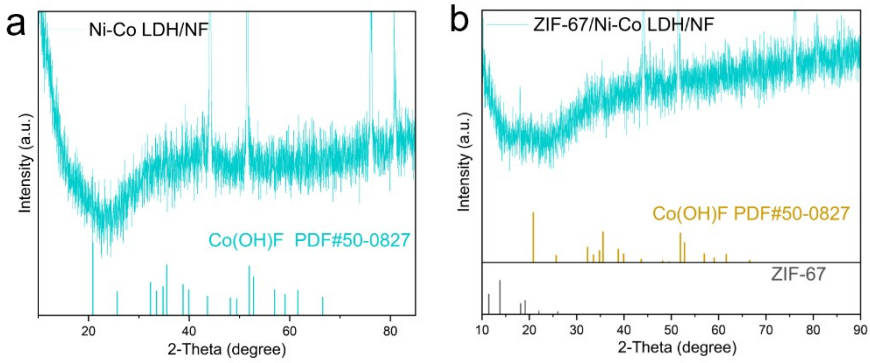

Fig. S2. XRD patterns of (a) Ni-Co LDH/NF, and (b) ZIF-67/Ni-Co LDH/NF intermediates.

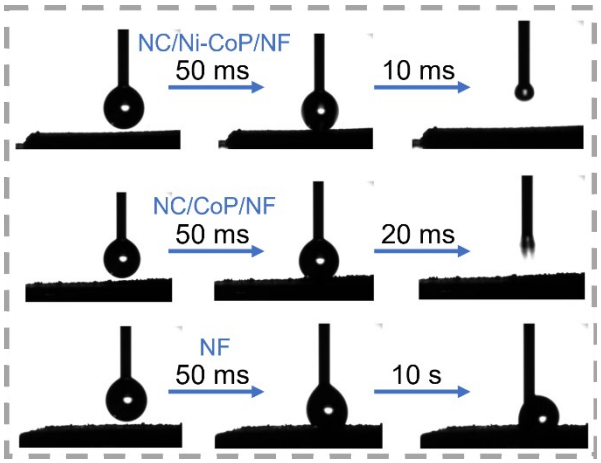

Fig. S3. Dynamic wettability behavior of NC/Ni-CoP/NF compared with NC/CoP/NF and bare NF.

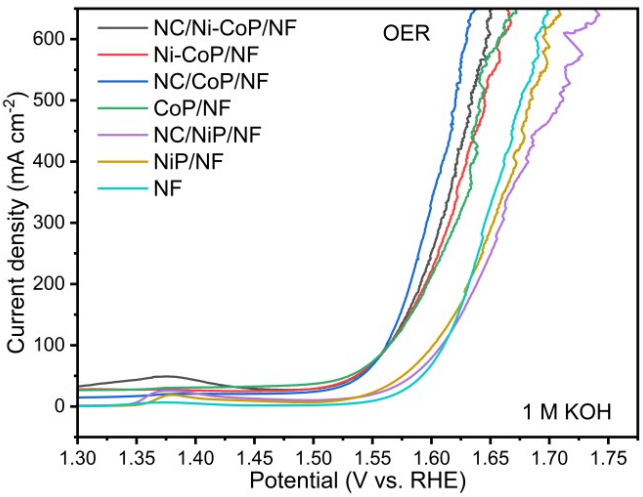

Fig. S4. OER polarization curves of NC/Ni-CoP/NF, Ni-CoP/NF, NC/CoP/NF, NC/NiP/NF, NiP/NF, and NF in 1 M KOH.

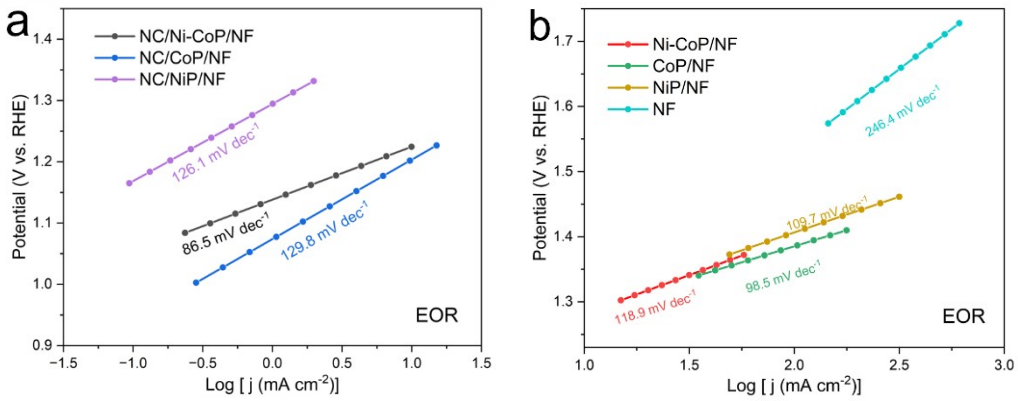

Fig. S5. Tafel plots of NC/Ni-CoP/NF, Ni-CoP/NF, NC/CoP/NF, CoP/NF, NC/NiP/NF, NiP/NF, and NF for EOR in 1 M KOH containing 1 M ethanol.

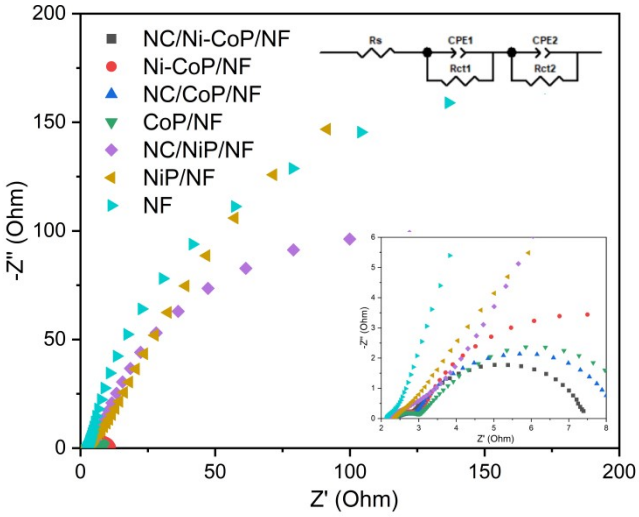

Fig. S6. Nyquist plots of NC/Ni-CoP/NF, Ni-CoP/NF, NC/CoP/NF, CoP/NF, NC/NiP/NF, NiP/NF, and NF for EOR; inset used in **Figure 2e**.

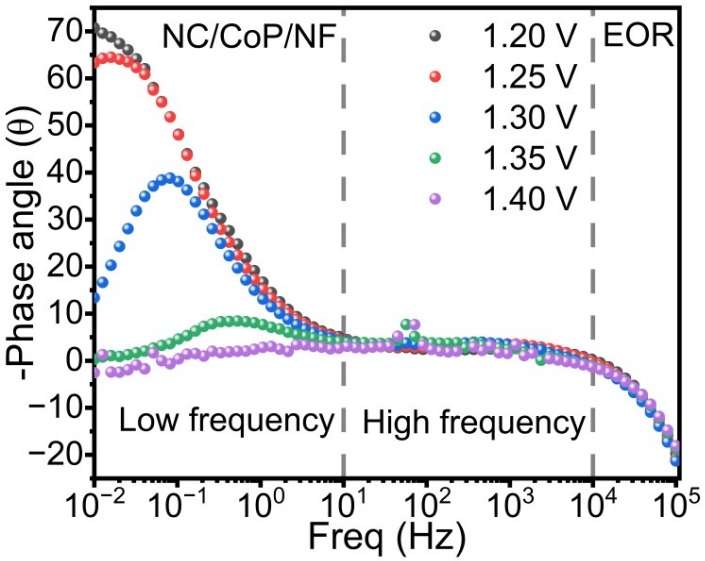

Fig. S7. Bode phase plot of NC/CoP/NF for comparison with **Fig. 2f–g**.

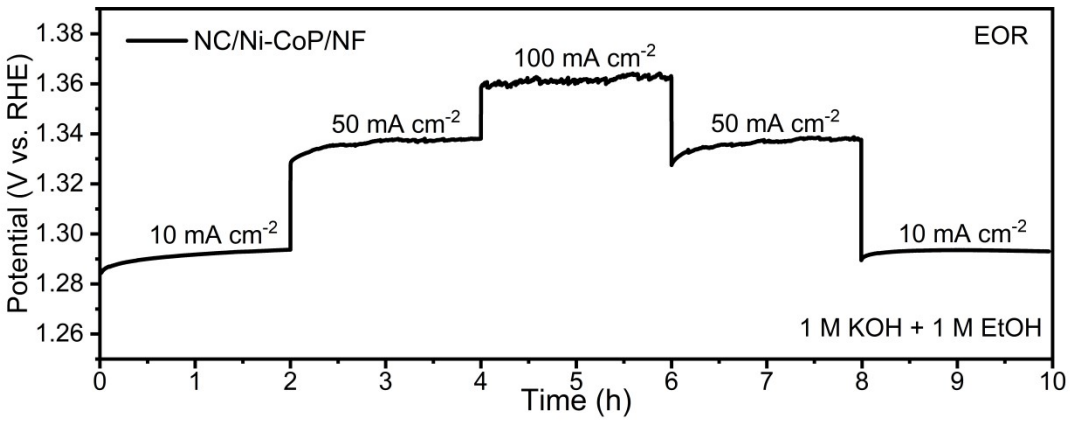

Fig. S8. Stepwise chronopotentiometric measurement at increasing current densities.

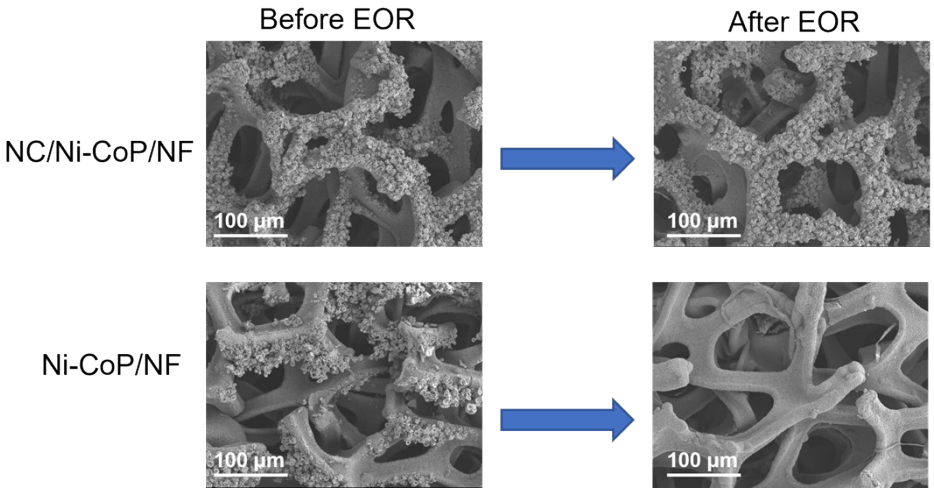

Fig. S9. Post-reaction SEM images of NC/Ni-CoP/NF and Ni-CoP/NF after EOR.

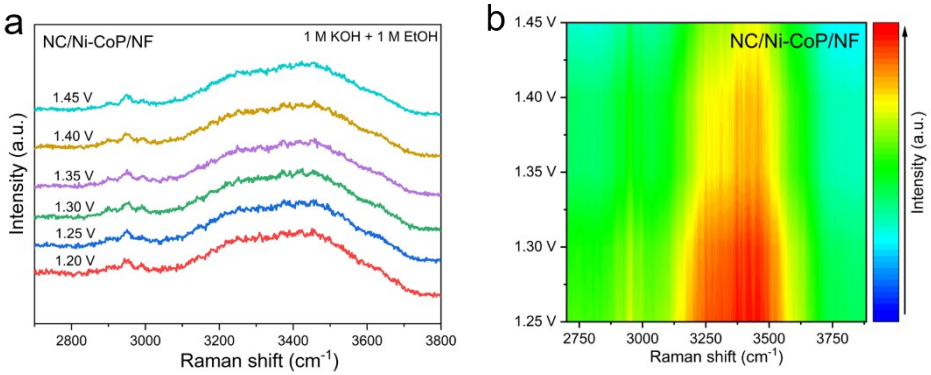

Fig. S10. (a) Potential-dependent Raman spectra of the O-H stretching region for NC/Ni-CoP/NF. (b) Corresponding contour map showing the evolution of hydrogen-bonding structures with increasing potential.

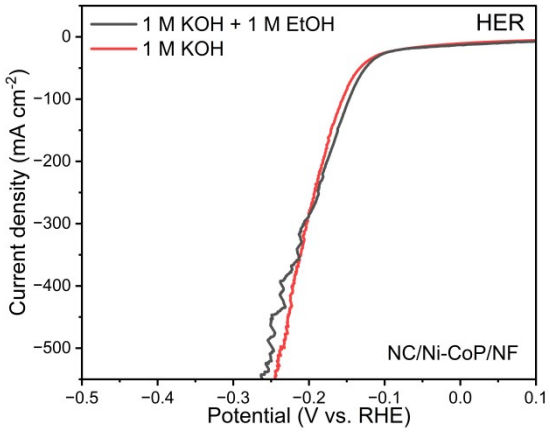

Fig. S11. HER curves of NC/Ni-CoP/NF in 1 M KOH and 1 M KOH containing 1 M EtOH.

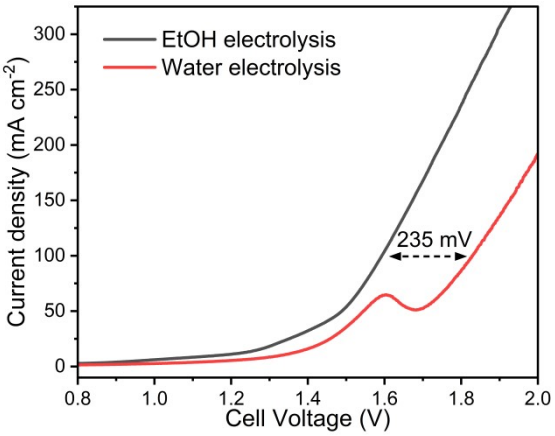

Fig. S12. LSV curves of bifunctional NC/Ni-CoP/NF in HER||EOR (EtOH electrolysis) and HER||OER systems (Water electrolysis).

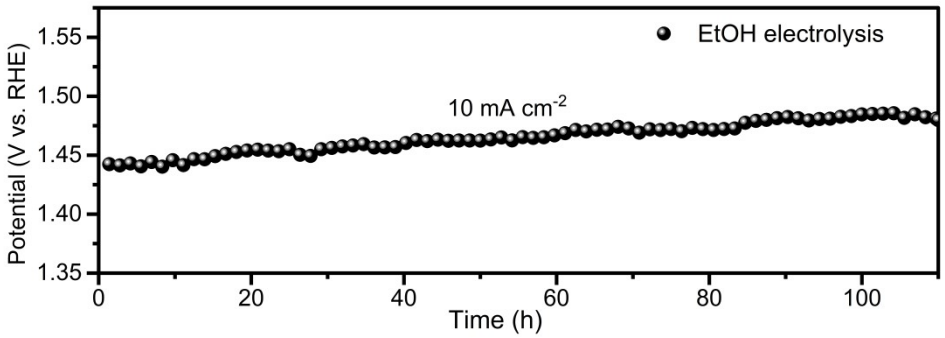

Fig. S13. Chronopotentiometric curves of bifunctional NC/Ni-CoP/NF system for HER||EOR electrolysis at 10 mA cm^{-2}.

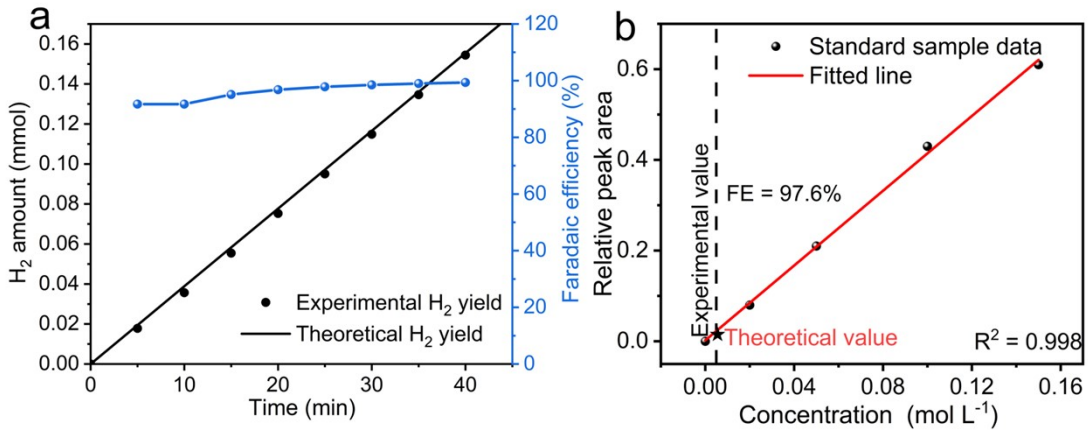

Fig. S14. (a) Faradaic efficiency of H_2 production at the cathode. (b) Faradaic efficiency of acetate production at the anode.

Tab. S1. Potentials required to achieve 100 and 500 mA cm^{-2} for NC/Ni-CoP/NF, Ni-CoP/NF, NC/CoP/NF, CoP/NF, NC/NiP/NF, NiP/NF, and NF during EOR in 1 M KOH containing 1 M ethan

Catalysts	Potential (V. vs RHE) @ 100 mA cm^{-2}	Potential (V. vs RHE) @ 500 mA cm^{-2}
NC/Ni-CoP/NF	1.35	1.44
Ni-CoP/NF	1.39	1.53
NC/CoP/NF	1.37	1.49
CoP/NF	1.38	1.51
NC/NiP/NF	1.39	1.47
NiP/NF	1.40	1.51
NF	1.46	1.70

Tab. S2. Comparison of electrocatalytic ethanol oxidation properties of Ni-CoP/NC/NF in terms of Tafel slope and current density at 10 mA cm^{-2} with other reported transition metal-based catalysts reported in the previous literature.

Catalysts	Electrolyte	Potential (V. vs RHE) @ 10 mA cm^{-2}	Tafel slope ($mV\ dec^{-1}$)	Ref.
VSe-$NiSe_2$@$CoSe_2$	1.0 M KOH + 1.0 M EtOH	1.33	63	[1]
$NiSe_2$@$CoSe_2$	1.0 M KOH + 1.0 M EtOH	1.42	99	[1]
ZIF67@$Ni(OH)_2$	1.0 M KOH + 1.0 M EtOH	1.40	104	[2]
$CoSe_2$@C	1.0 M KOH + 1.0 M EtOH	1.44	74	[3]
Ni-O(OH)	1.0 M KOH + 1.0 M EtOH	1.37	39	[4]
$Co(OH)_2$@$Ni(OH)_2$	1.0 M KOH + 1.0 M EtOH	1.30	55	[5]
$Ni(OH)_2$	1.0 M KOH + 1.0 M EtOH	1.40	96	[5]
Ni-doped ZIF-67	1.0 M KOH + 1.0 M EtOH	1.55	193	[5]
NiCuSe	1.0 M KOH + 1.0 M EtOH	1.42	230	[6]
CoS_2/CC	1.0 M KOH + 1.0 M EtOH	1.40	133	[7]
NC/Ni-CoP/NF	**1.0 M KOH + 1.0 M EtOH**	**1.24**	**86.5**	**This work**

References

1. Li J, Fang F, Jian Y, et al. Modulation of Se vacancies on $NiSe_2$@$CoSe_2$ heterostructures to optimize ethanol electrooxidation activity for efficient hybrid water splitting and zinc-ethanol-air batteries. *Inorg. Chem. Front.* 2025, 12(17): 5029-5036.
2. Zhu J, Li Z, Li J, et al. Mixed-solvent solvothermal synthesis of metal-organic framework-supported nickel hydroxide toward a novel lattice oxygen-mediated ethanol oxidation pathway. *Appl. Catal. B Environ. Energy* 2025, 382: 126008.
3. Ning S, Jian Y, Yu G Q, et al. Dynamic Electron Spring Effect in Hollow Fe_2O_3/$CoSe_2$ Heterostructure Enhance Ethanol Electro-Oxidation Activity and Stability. *Adv. Funct. Mater.* 2025, 35(48): 2509007.
4. Xu W, Shang Q, Sun B, et al. Highly Active Electrocatalytic Alcohol Oxidation Coupled Hydrogen Production with Unsaturated Ni-O(OH) Coordination. *Adv. Energy Mater.* 2026, 16(1): e70448.
5. Li Z, Ning S, Xu J, et al. In situ electrochemical activation of $Co(OH)_2$@$Ni(OH)_2$ heterostructures for efficient ethanol electrooxidation reforming and innovative zinc–ethanol–air batteries. *Energy Environ. Sci.* 2022, 15(12): 5300-5312.
6. Li X, Chen M, Ye Y, et al. Electronic Structure Modulation of Nickel Sites by Cationic Heterostructures to Optimize Ethanol Electrooxidation Activity in Alkaline Solution. *Small*. 2023,19(18):2207086.
7. Sheng S, Ye K, Sha L, et al. Rational design of Co-S-P nanosheet arrays as bifunctional electrocatalysts for both ethanol oxidation reaction and hydrogen evolution reaction. *Inorg. Chem. Front*. 2020, 7(22):4498-4506.